IEEE Access
Multidisciplinary ⋮ Rapid Review ⋮ Open Access Journal

Received 11 July 2023, accepted 17 August 2023, date of publication 25 August 2023, date of current version 26 September 2023.

Digital Object Identifier 10.1109/ACCESS.2023.3308823

RESEARCH ARTICLE

Design of Neuro Fuzzy Sliding Mode Controller for Active Magnetic Bearing Control System

HAREGEWOYN FENTAW ASRES[1] **AND ABRHAM TADESSE KASSIE**[2]
[1]School of Electrical and Computer Engineering, Woldia Institute of Technology, Woldia University, Woldia 7220, Ethiopia
[2]Faculty of Electrical and Computer Engineering, Bahir Dar Institute of Technology, Bahir Dar University, Bahir Dar 6000, Ethiopia
Corresponding author: Abrham Tadesse Kassie (abrham2048@gmail.com)

ABSTRACT Active Magnetic Bearing system (AMB) is a nonlinear mechatronic device utilized for levitating the rotating components of a machine without physical contact with the stationary parts. The nonlinearity properties pose a challenge for ensuring system stability. To achieve stable and optimal performance, controllers must be incorporated. A model of the proposed AMB has been derived and results a 2×2 MIMO system. To simplify it, the model is linearized using Taylor series expansion technique. Simulation experiments have been conducted using MATLAB. In this paper, a neuro-fuzzy sliding mode controller (NFSMC) has been designed to control the position of the AMB system. Simulink models of the AMB with different control strategies have been developed for conducting simulation studies. The comparison results indicate that, with SMC, the position of the rotors follows the reference input but it is affected by chattering. It is further observed that FSMC reduces the chattering, while NFSMC controllers automatically eliminate the chattering problem and operate more robustly and smoothly. The system's stability has been analyzed using the Lyapunov theorem. According to the results gained, the NFSMC improves the overall system performance. The NFSMC controller yields an optimal result having no overshoot, a settling time of 0.5 sec, and a rise time of 0.10 sec in comparison with FSMC controller which exhibits overshoot of 0.392%, a settling time of 0.75 sec, and a rise time of 0.133 sec, while the SMC shows overshoot of 9.047%, a settling time of 7.5 sec, and a rise time of 0.17 sec.

INDEX TERMS AMB, NN, fuzzy logic, SMC, MATLAB.

I. INTRODUCTION

Bearings are essential components of a mechanical system. They fulfill the function of constraining the relative motion of a mechanical structure to the intended motion while minimizing friction between the moving and stationary parts. In various mechanical structures and machines, bearings enable unrestricted linear or rotational movement around a fixed axis or control the normal forces acting on moving parts to prevent motion. Bearings come in numerous types, which are categorized based on their operational characteristics, permissible motions, or the directions of applied loads. Among these various types, ball bearings are first invented and most widely used [1]. Magnetic bearings can be classified as AMBs and PMB (Passive Magnetic Bearings). PMBs consist of permanent magnets and do not require electrical power, whereas active magnetic bearings are constructed using electromagnets. They allow the output flux to be adjusted by modifying the current on the coil. In numerous applications, AMBs are replacing oil-lubricated bearings due to several advantages. These advantages encompass enhanced reliability through decreased maintenance requirements, minimized frictional losses, absence of contamination, reduced machine vibration, and improved health monitoring and diagnostic capabilities. By employing magnetic bearings in rotating machinery, these benefits can be achieved.

Despite the numerous benefits they offer, the utilization of magnetic bearings has historically been limited due to factors such as their size, complexity of integration with machines, the need for a substantial external control system, and high costs. However, recent advancements in magnetic bearing technology have addressed many of these limitations,

The associate editor coordinating the review of this manuscript and approving it for publication was Zhuang Xu.

resulting in downsizing, simplified integration, and reduced costs. As a result, magnetic bearings are now replacing oil-lubricated bearings in various new machine types across multiple sectors. The AMB system levitates and stabilizes the rotating shaft by applying regulated electromagnetic forces to the rotor in both the radial and axial axes. The principle of magnetic suspension, implemented through AMBs, is predominantly utilized [2]. AMB offers several advantages over traditional ball or journal bearings. The primary benefit lies in its ability to suspend a rotor within a magnetic field, enabling it to achieve high speeds of up to 60,000 RPM without any physical contact with mechanical components. In an AMB system, only windage friction is present, which can be completely eliminated when the device operates within a vacuum enclosure. Apart from the reduction in energy loss and the elimination of lubrication systems, this frictionless characteristic of AMB contributes to its extended lifespan. AMB exhibits resistance to pressure and temperature variations, as well as minimal equipment wear, further enhancing its durability. The rapid rotation of the rotor and the narrow air gap between the rotor and the stator pose a significant challenge in maintaining the rotor's equilibrium position. Any deviation from this position can lead to serious consequences, such as the rotor coming into contact with the stator and the failure of the operation. Therefore, a critical concern lies in effectively regulating the rotor position in AMB systems [3].

SMC is employed to attain both high robustness and rapid response. But it often faces challenges related to the undesirable chattering effect. To address this issue, two intelligent algorithms are utilized in the design of the SMC to automatically mitigate the chattering effect. This paper proposes the design of a NFSMC for controlling the position and current of an AMB system. The NFSMC offers advantages over conventional SMC. The aim of the controller is to maintain levitation and ensure that the rotor position stays centered within the stator. AMB controllers need to adhere to various standards, including ensuring system robustness, employing high gain, and accurately measuring the rotor's position. In [4], a Unity SMC for an AMB system is presented. The article utilizes a linearized uncertain model of AMBs to construct a nonlinear SMC and a Lyapunov function for the electromechanical system. To facilitate the controller's operation, measurements of rotor displacement and its derivatives are essential. The suggested controller achieves finite-time regulation due to its employment of a discontinuous control rule. However, it suffers from a flaw known as the chattering problem. In [5], a Second-Order SMC for an AMB are proposed, while [6] discusses the utilization of sliding mode approaches for design and analysis of an AMB system. The controllers proposed in these studies are based on a linearized model of the magnetic bearing around the balanced position. It is crucial to note that the AMB's performance may be affected when significant changes occur in the system's operating conditions, such as during high-speed rotation or under the impact of a heavy load. In [7], an AMB System using SMC with Neural Network (NN) is developed. The controller combines SMC with NN to address the nonlinearity and uncertainty of the AMB system while meeting accuracy and robustness requirements. The paper's main contribution lies in the utilization of a one-layer NN to account for unmodeled uncertainties in the system. Additionally, [8] demonstrates an AMB system based on a fuzzy basis function neural network (RFBFNN). The publication in [9] presents the design and stability analysis of the NFSMC. In these studies, NN is employed to estimate an ideal sliding surface, while a fuzzy logic system is utilized to construct a nonlinear sliding surface. Furthermore, [10] suggests a sliding-mode technique for developing a dependable neuro-fuzzy controller. This article introduces the novel use of a neuro-fuzzy network to approximate the ideal controller online. Additionally, the Taylor linearization method is applied to enhance the controller's learning capability. In [11], a NFSMC is proposed for the Coupled Tanks System. The primary objectives of this paper are to address and eliminate the chattering issue typically associated with SMC, as well as to offer solutions for computing the equivalent control involved in the system.

Here the author proposes to design NFSMC for AMB system by combining NN and fuzzy logic systems with conventional SMC. A feedforward NN is employed to analyze the equivalent controller, while fuzzy logic is utilized to compute the switching functions. The parameters have been updated through an offline tuning system.

The paper is organized in five main sections. The first section provides the detailed introduction and literature review about the proposed system. Section II presents the mathematical model of the AMB system. The proposed controller design has been derived and discussed in Section III. Section IV addresses the results gained from the simulation with their respective discussions. Finally, the conclusion has been given in section V.

II. AMB SYSTEM MODELING

The AMB system consists of three essential components: the power amplifier, electromagnetic actuator, and rotor, as depicted in Fig. 1.

A. MODELING OF THE AMB ACTUATOR

The magnetic force in the AMB is generated when the current flows through the coils of the electromagnetic actuators. This current signal is transmitted from the power amplifiers to the actuators. The magnetic force allows the rotor to be suspended above the stator without any physical contact. This force not only counteracts the weight of the rotor but also compensates for additional disturbance forces. The current-induced magnetic field creates an upward thrust. The equation below, derived from Ampere's loop law, incorporates the magnetic field (H), which comprises the flux density (B), the number of segments across the path (ns) when H is constant, and the potential number of coil types (nc) [3].

$$\sum_{i=1}^{n_s} H_i l_i = \sum_{i=1}^{n_c} N_i I_i \tag{1}$$

where, I, N, and, l represents coil current, number of coils, and length of the path respectively.

Under the assumption that the permeability (μ) of the mediums remains constant in every individual segment, the flux density can be expressed as follows:

$$B_i = \mu_i H_i \tag{2}$$

Then combine (1) and (2) yields equation (3)

$$\sum_{i=1}^{n_s} \frac{B_i l_i}{\mu_i} = \sum_{i=1}^{n_c} N_i I_i \tag{3}$$

According to Fig.1, r, u, i, f, x and y represent desired displacement, control input, coil current, magnetic force, actual displacement and feedback signal respectively.The detaield explanation of the blocks in Fig. 1 has been given in section II.

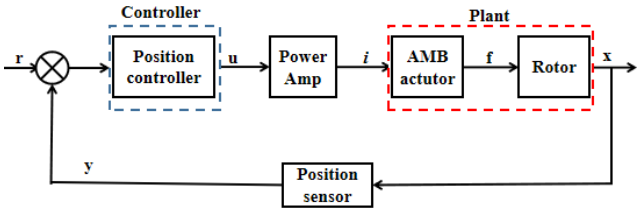

FIGURE 1. AMB control system.

By assuming the permeability of air (μ_g) is much less than that of iron (μ_0), the terms $\frac{Bl_0}{\mu_0}$ can be neglected, where l_0 means the length of the magnetic flux path in the core.

The stored energy and electromagnetic force are given in equations (4) to (6).

$$2\frac{\mathrm{B_g g}}{\mu_\mathrm{g}} = \mathrm{NI} \tag{4}$$

$$\mathrm{E} = \frac{1}{2}(\mathrm{B_g H_g A 2 x_0}) \tag{5}$$

$$\mathrm{F} = \frac{1}{\mu_0}\mathrm{A}\left(\frac{\mu_0 \mathrm{NI}}{2\mathrm{x_0}}\right)^2 = \frac{\mu_0 \mathrm{N^2 I^2 A}}{4\mathrm{x_0^2}}\cos\alpha \tag{6}$$

A simplified form of equation (6), the air gap distance, and control current becomes.

$$x_+ = x_0 + \mathrm{x} \tag{7a}$$

$$x_- = x_0 - \mathrm{x} \tag{7b}$$

$$\mathrm{i_+} = \mathrm{i_0} + \mathrm{i_x} \quad \text{and } \mathrm{i_-} = \mathrm{i_0} - \mathrm{i_x} \tag{7c}$$

$$F = f_+ - f_- = \frac{\mu A N^2}{4}\left[\frac{(i_0 + i_x)^2}{(x_o + x)^2} - \frac{(i_o - i_x)^2}{(x_o - x)^2}\right]\cos\alpha \tag{8}$$

$$\mathrm{F} = \mathrm{k}\left[\frac{(i_0 + i_x)^2}{(x_o + x)^2} - \frac{(i_o - i_x)^2}{(x_o - x)^2}\right] \tag{9}$$

where $\mathrm{k} = \frac{1}{4}\mu_0 A N^2 \cos\alpha$, and x, F, x_o, m, μ, A, and N, represents displacement of the rotor relative to the equilibrium position, magnetic force which is an opposite direction compared to x, nominal air gap, mass of rotor, vacuum magnetic permeability, pole area of the electromagnet, and number of turns respectively. By making a Taylor series expansion to equation (9) in the vicinity of the equilibrium point and eliminate the higher order equation we get;

$$\mathrm{F} = 4\mathrm{k}\frac{\mathrm{i_0^2}}{\mathrm{x_0^2}}\left[\frac{\mathrm{i_x}}{\mathrm{i_0}} - \frac{\mathrm{x}}{\mathrm{x_0}}\right] \tag{10}$$

Linearize equation (10) around the equilibrium point yields equation (11).

$$F = k_i i_x + k_x x$$
$$k_i = 4\mathrm{k}\frac{\mathrm{i_0}}{\mathrm{x_0^2}} \quad \text{and } k_x = -4\mathrm{k}\frac{\mathrm{i_0^2}}{\mathrm{x_0^3}} \tag{11}$$

where, k_i is the current stiffness and k_x is the displacement stiffness

B. MODELING OF THE RIGID ROTOR

The rotor mass system is supported by radial AMBs, while the axial support is not taken into account. As a result, the coupling effect between axial and radial dynamics is neglected. The rotor is assumed to be a rigid rotor influenced by the magnetic levitation force. This method reduces the coupling between radial motions in two perpendicular planes, allowing for the calculation of motion in a single plane. In this regard, a rigid beam model can precisely describe the radial motion occurring within this plane, which encompasses the displacement of the rotor and its rotation around an axis passing through gravity center [2].

For the sake of simplicity, the gyroscopic effect is neglected, and the influence of gravity on the rotor is disregarded [12]. The forces and displacements affecting the rotor are determined along the X and Y planes.

The term 'a' and 'b,' in Fig. 2, separates the two bearings called bearing A and bearing B from the center of gravity of the rotor. The model for rotor mass system can be found easily by combining the electromagnetic actuator model with rotor mathematical equations. Therefore, we can obtain the equation by using Newton second law:

$$\mathrm{M}\ddot{x} = F + F_d \tag{12}$$

where: F = electromagnetic force, F_d = disturbance force.

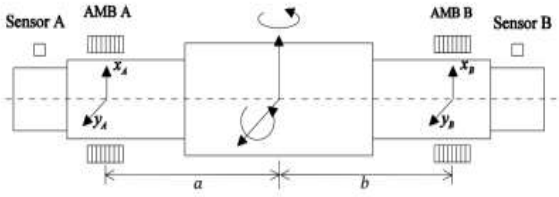

FIGURE 2. Schematic view of AMB rotor mass system [12].

Assume ignoring the disturbance force, combine equation (11) and (12) we get

$$\mathrm{M}\ddot{x} = k_i i_x + k_x x$$

$$\mathrm{M} = \begin{bmatrix} \mathrm{m_1} & \mathrm{m_3} \\ \mathrm{m_3} & \mathrm{m_2} \end{bmatrix} \tag{13}$$

where

$$\mathrm{m_1} = \frac{\mathrm{m} * \mathrm{b}^2 + \mathrm{I_r}}{(\mathrm{a}+\mathrm{b})^2} \tag{14a}$$

$$\mathrm{m_2} = \frac{\mathrm{m} * \mathrm{a}^2 + \mathrm{I_r}}{(\mathrm{a}+\mathrm{b})^2} \tag{14b}$$

$$\mathrm{m_3} = \frac{\mathrm{m} * \mathrm{a} * \mathrm{b} - \mathrm{I_r}}{(\mathrm{a}+\mathrm{b})^2} \tag{14c}$$

The terms 'a' and 'b' in equation (14) stand for the AMBs' distance from the rotor's center of gravity. *Ir* is the rotor radial moment of inertia. In this work, it is assumed that the rotor's center of gravity lies in the middle of its axial length. As a result, the lengths of 'a' and 'b' are equal [13]. Using the nonlinear force, the non-linear model becomes:

$$\begin{bmatrix} \ddot{x}_a \\ \ddot{x}_b \end{bmatrix} = M^{-1} * \begin{bmatrix} f\,(x_a, i_a) \\ f\,(x_b, i_b) \end{bmatrix} \tag{15}$$

$$f\,(x_a, i_a) = k\frac{i_a^2}{x_a^2} \tag{16a}$$

$$f\,(x_b, i_b) = k\frac{i_b^2}{x_b^2} \tag{16b}$$

$$\begin{aligned} \ddot{x_a} &= \frac{m_2}{m_1 m_2 - m_3^2} f\,(x_a, i_a) \\ &\quad - \frac{m_3}{m_1 m_2 - m_3^2} f\,(x_b, i_b) \\ &= \frac{m_2 k}{m_1 m_2 - m_3^2}\frac{i_a^2}{x_a^2} - \frac{m_3 k}{m_1 m_2 - m_3^2}\frac{i_b^2}{x_b^2} \end{aligned} \tag{17}$$

$$\begin{aligned} \ddot{x_b} &= \frac{-m_3}{m_1 m_2 - m_3^2} f(x_a, i_a) + \frac{m_1}{m_1 m_2 - m_3^2} f(x_b, i_b) \\ &= \frac{-m_3 k}{m_1 m_2 - m_3^2}\frac{i_a^2}{x_a^2} + \frac{m_1 k}{m_1 m_2 - m_3^2}\frac{i_b^2}{x_b^2} \end{aligned} \tag{18}$$

After rearranging terms, rewriting and combining equation (17) and Equation (18) in matrix form results in equation (19).

$$\begin{aligned} \begin{bmatrix} \ddot{x}_a \\ \ddot{x}_b \end{bmatrix} &= \frac{1}{2}\begin{bmatrix} \frac{m_2}{m_1 m_2 - m_3^2} k\frac{i_a^2}{x_a^3} & \frac{-m_3}{m_1 m_2 - m_3^2} k\frac{i_b^2}{x_b^3} \\ \frac{-m_3}{m_1 m_2 - m_3^2} k\frac{i_a^2}{x_a^3} & \frac{m_1}{m_1 m_2 - m_3^2} k\frac{i_b^2}{x_b^3} \end{bmatrix}\begin{bmatrix} x_a \\ x_b \end{bmatrix} \\ &\quad + \frac{1}{2}\begin{bmatrix} \frac{m_2}{m_1 m_2 - m_3^2} k\frac{i_a}{x_a^2} & \frac{-m_3}{m_1 m_2 - m_3^2} k\frac{i_b}{x_b^2} \\ \frac{-m_3}{m_1 m_2 - m_3^2} k\frac{i_a}{x_a^2} & \frac{m_1}{m_1 m_2 - m_3^2} k\frac{i_b}{x_b^2} \end{bmatrix}\begin{bmatrix} i_a \\ i_b \end{bmatrix} \end{aligned} \tag{19}$$

$$\begin{bmatrix} \ddot{x}_a \\ \ddot{x}_b \end{bmatrix} = \frac{1}{2}\begin{bmatrix} a\frac{i_a^2}{x_a^3} & b\frac{i_b^2}{x_b^3} \\ b\frac{i_a^2}{x_a^3} & c\frac{i_b^2}{x_b^3} \end{bmatrix}\begin{bmatrix} x_a \\ x_b \end{bmatrix} + \frac{1}{2}\begin{bmatrix} a\frac{i_a}{x_a^2} & b\frac{i_b}{x_b^2} \\ b\frac{i_a}{x_a^2} & c\frac{i_b}{x_b^2} \end{bmatrix}\begin{bmatrix} i_a \\ i_b \end{bmatrix} \tag{20}$$

where,

$$\begin{aligned} a &= \frac{m_2}{m_1 m_2 - m_3^2} k, \\ b &= \frac{m_3}{m_1 m_2 - m_3^2} k, \\ c &= \frac{m_1}{m_1 m_2 - m_3^2} k \end{aligned} \tag{21}$$

The linearized model is, based on the linearized force in equation (11), derived as:

$$\begin{aligned} \begin{bmatrix} \ddot{x}_a \\ \ddot{x}_b \end{bmatrix} &= M^{-1}\begin{bmatrix} k_{xa} & 0 \\ 0 & k_{xb} \end{bmatrix}\begin{bmatrix} x_a \\ x_b \end{bmatrix} + M^{-1}\begin{bmatrix} k_{ia} & 0 \\ 0 & k_{ib} \end{bmatrix}\begin{bmatrix} i_a \\ i_b \end{bmatrix} \\ \begin{bmatrix} \ddot{x}_a \\ \ddot{x}_b \end{bmatrix} &= \begin{bmatrix} \frac{\mathrm{m_2}}{\mathrm{m_1 m_2 - m_3^2}}\mathrm{k_{xa}} & \frac{-\mathrm{m_3}}{\mathrm{m_1 m_2 - m_3^2}}\mathrm{k_{xb}} \\ \frac{-\mathrm{m_3}}{\mathrm{m_1 m_2 - m_3^2}}\mathrm{k_{xa}} & \frac{\mathrm{m_1}}{\mathrm{m_1 m_2 - m_3^2}}\mathrm{k_{xb}} \end{bmatrix}\begin{bmatrix} \mathrm{x_a} \\ \mathrm{x_b} \end{bmatrix} \\ &\quad + \begin{bmatrix} \frac{\mathrm{m_2}}{\mathrm{m_1 m_2 - m_3^2}}\mathrm{k_{ia}} & \frac{-\mathrm{m_3}}{\mathrm{m_1 m_2 - m_3^2}}\mathrm{k_{ib}} \\ \frac{-\mathrm{m_3}}{\mathrm{m_1 m_2 - m_3^2}}\mathrm{k_{ia}} & \frac{\mathrm{m_1}}{\mathrm{m_1 m_2 - m_3^2}}\mathrm{k_{ib}} \end{bmatrix}\begin{bmatrix} \mathrm{i_a} \\ \mathrm{i_b} \end{bmatrix} \end{aligned} \tag{22}$$

State space representation of the above system becomes

$$\begin{aligned} \begin{bmatrix} \dot{\mathrm{x}}_1 \\ \dot{\mathrm{x}}_2 \\ \dot{\mathrm{x}}_3 \\ \dot{\mathrm{x}}_4 \end{bmatrix} &= \begin{bmatrix} 0 & 1 & 0 & 0 \\ \frac{\mathrm{m_2}}{\mathrm{m_1 m_2 - m_3^2}}\mathrm{k_{xa}} & 0 & \frac{-\mathrm{m_3}}{\mathrm{m_1 m_2 - m_3^2}}\mathrm{k_{xb}} & 0 \\ 0 & 0 & 0 & 1 \\ \frac{-\mathrm{m_3}}{\mathrm{m_1 m_2 - m_3^2}}\mathrm{k_{xa}} & 0 & \frac{\mathrm{m_1}}{\mathrm{m_1 m_2 - m_3^2}}\mathrm{k_{xb}} & 0 \end{bmatrix}\begin{bmatrix} \mathrm{x_1} \\ \mathrm{x_2} \\ \mathrm{x_3} \\ \mathrm{x_4} \end{bmatrix} \\ &\quad + \begin{bmatrix} 0 & 0 \\ \frac{\mathrm{m_2}}{\mathrm{m_1 m_2 - m_3^2}}\mathrm{k_{ia}} & \frac{-\mathrm{m_3}}{\mathrm{m_1 m_2 - m_3^2}}\mathrm{k_{ib}} \\ 0 & 0 \\ \frac{-\mathrm{m_3}}{\mathrm{m_1 m_2 - m_3^2}}\mathrm{k_{ia}} & \frac{\mathrm{m_1}}{\mathrm{m_1 m_2 - m_3^2}}\mathrm{k_{ib}} \end{bmatrix}\begin{bmatrix} \mathrm{u_a} \\ \mathrm{u_b} \end{bmatrix} \\ \mathrm{y} &= \begin{bmatrix} 1 & 0 & 0 & 0 \\ 0 & 0 & 1 & 0 \end{bmatrix}\begin{bmatrix} x_1 \\ x_2 \\ x_3 \\ x_4 \end{bmatrix} \end{aligned} \tag{23}$$

The proposed system model has been finalized as a MIMO system having a 2 × 2 input-output relationships.

C. MODELING OF THE AMPLIFIER

The controller sends a voltage signal to the amplifier model, which in turn sends a current signal to the actuator coil. Usually, the current control is purely proportional. The following transfer function is calculated in [14] under the presumption that the inductance L is constant and the coil resistance RC

is minimal.

$$G_a(s) = \frac{k_p}{sL + (k_p + RC)} = \frac{k_p}{sL + k_p} \tag{24}$$

Consequently, k_p is the amplifier's proportionate gain and is strongly influenced by the band-width, which is represented by ω. The power amplifier does not only amplify the current but also filters out the high frequency components of the current signal. Therefore, the power amplifier also acts as a low pass filter.

$$\mathrm{G_a}(s) = \frac{\omega_{bw}}{s + \omega_{bw}} \tag{25}$$

where, $\omega_{bw} = \frac{k_p}{L}$.

To find out bandwidth of the power amplifier, first the maximum magnetic force that can be produced, the maximum power output of the amplifier and the air gap must be identified.

Once the required parameters are identified we can directly calculate the bandwidth of the amplifier.

$$\omega_{bw} = \frac{P_{max} * cos(a)}{X_0 * F_{max}} \tag{26}$$

where, a is considered as the angle between consecutive poles of the electromagnetic actuators. Assuming that the AMB System being discussed here has four actuators and each having two poles.

$$\begin{aligned} \mathrm{F_{max}} &= \mathrm{K_i} * \mathrm{i_{max}} + \mathrm{K_S} * \mathrm{X_{max}} \\ \mathrm{i_{max}} &= 2 * \mathrm{i_0} \quad \text{and } \mathrm{X_{max}} = 2 * \mathrm{X_0} \end{aligned} \tag{27}$$

where: Ki-is Current stiffness constant of the electromagnetic actuator, KS-is Position stiffness constant of the electromagnetic actuator

The transfer function of amplifier models in equation (24) will be:

$$\mathrm{G_a}(s) = \frac{I(s)}{u(s)} = \frac{\omega_{bw}}{s + \omega_{bw}} \tag{28}$$

MIMO state space forms of the amplifier model becomes;

$$\begin{bmatrix} \dot{i_a} \\ \dot{i_b} \end{bmatrix} = \begin{bmatrix} -\omega_{bw} & 0 \\ 0 & -\omega_{bw} \end{bmatrix} \begin{bmatrix} i_a \\ i_b \end{bmatrix} + \begin{bmatrix} \omega_{bw} & 0 \\ 0 & \omega_{bw} \end{bmatrix} \begin{bmatrix} u_a \\ u_b \end{bmatrix} \tag{29}$$

The interaction of various inputs and outputs is one of the trickiest parts of controlling MIMO systems. Every system output will be impacted by every input. Thus, in AMB control system, a control action on bearing A will have an impact on the position of the rotor at bearing A as well as bearing B, and vice versa. In order to approach this MIMO control design problem as multiple SISO control design problems, we should either decouple the system using decoupling techniques or justify that the system is already decoupled. When the non-diagonal components of the square transfer matrix functions are zero, the MIMO system is completely decoupled. In other terms, the system is said to be decoupled if the transfer matrix is a diagonal matrix [15]. As it can be observed

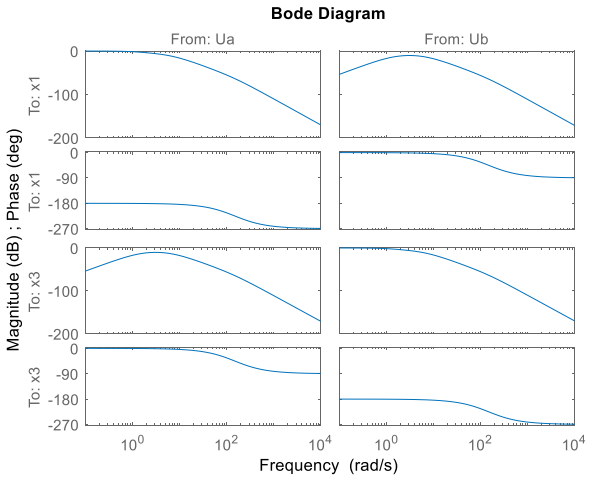

FIGURE 3. Bode plot of open loop AMB system.

from the bode plots in Fig. 3, the magnitude of the two main diagonal transfer functions of the transfer matrix is greater than the off-diagonal elements at lower frequencies. This shows that the AMB is diagonally dominant plant. By taking into account each input-output pair separately, a good controller can be designed if a transfer matrix is diagonally dominant.

The right pairing of the input and output is a crucial consideration in the controller design. The relative gain array (RGA) is one method of pairing selection. The RGA will display the degree of process interaction and provide information on the connections between control loops [15].

The model of the AMB system is given by the state-space representation as in equation (23). it can be represented by a 2×2 transfer matrix function G(s) given as:

$$\begin{aligned} G(s) &= \begin{bmatrix} G_{11}(s) & G_{12}(s) \\ G_{21}(s) & G_{22}(s) \end{bmatrix} \\ \mathrm{RGA(G)} &= \Lambda(\mathrm{G}) \triangleq G(0) .* G^{-1}(0)^T \end{aligned} \tag{30}$$

where, '$*$' denotes elementwise multiplication

For the AMB system with transfer matrix given in equation (30) the RGA is calculated as:

$$\Lambda(\mathrm{G}) = \begin{bmatrix} \lambda_{11} & \lambda_{12} \\ \lambda_{21} & \lambda_{22} \end{bmatrix} = \begin{bmatrix} \lambda_{11} & 1 - \lambda_{11} \\ 1 - \lambda_{11} & \lambda_{11} \end{bmatrix} \tag{31}$$

$$\lambda_{11} = \frac{1}{1 - \frac{G_{12}(0)G_{21}(0)}{G_{11}(0)G_{22}(0)}} \tag{32}$$

Evaluating G (0) from equation (30), we get $\lambda 11$ to be

$$\lambda_{11} = 1$$

Hence, the RGA becomes:

$$\Lambda(\mathrm{G}) = \begin{bmatrix} 1 & 0 \\ 0 & 1 \end{bmatrix}$$

From the RGA result obtained above $\lambda 11 = \lambda 22 = 1$ designates coupled interaction has not effect on the pairing of input 1 with output 1 and input 2 with output 2. On the other

hand, the results $\lambda 12 = \lambda 21 = 0$ indicate that the output 1 with input 2 and output 2 with input 1 are loosely related. It is a clear indication that we cannot control output 1 and output 2 using the input 2 and input 1 respectively.

III. CONTROLLER DESIGN FOR AMB SYSTEM

SMC design can be completed into three key steps that are highly dependent on each other. These steps include: Surface selection, establishment of conditions for convergence, and determination of the control law. The characteristics of the system are solely influenced by the properties of the sliding surface. Therefore, designing the sliding surface is essential to achieve the desired system properties during sliding [16]. Let as define

$e = x_d - x$ -is the tracking error in the variable x and let $e = x_d - x = \left[e, \dot{e}, \ddot{e}, \ldots e^{n-1}\right]^T$ be the tracking error vector and the sliding surface are defined as;

$$S(x) = \left(\frac{d}{dt} + c\right)^{n-1} e(x) \tag{33}$$

where e(x) is the tracking error, c is a positive parameter and n is relative degree of the system.

In this paper, the first step involves designing SMC for the proposed system. Thus, Equation (22) and (29) are rewritten as:

$$\left.\begin{aligned} \dot{i}_a &= -\omega_{bw} i_a + \omega_{bw} u_a \\ \dot{i}_b &= -\omega_{bw} i_b + \omega_{bw} u_b \end{aligned}\right\} \tag{34}$$

$$\left.\begin{aligned} \ddot{x}_a &= \frac{m_2}{m_1 m_2 - m_3^2} k_{sa} x_a \\ &- \frac{m_3}{m_1 m_2 - m_3^2} k_{sb} x_b + \frac{m_2}{m_1 m_2 - m_3^2} k_{ia} i_a \\ &- \frac{m_3}{m_1 m_2 - m_3^2} k_{ib} i_b \\ \ddot{x}_b &= \frac{-m_3}{m_1 m_2 - m_3^2} k_{sa} x_a + \frac{m_1}{m_1 m_2 - m_3^2} k_{sb} x_b \\ &- \frac{m_3}{m_1 m_2 - m_3^2} k_{ia} i_a + \frac{m_1}{m_1 m_2 - m_3^2} k_{ib} i_b \end{aligned}\right\} \tag{35}$$

The tracking error and its rate of change are defined as:

$$\left.\begin{aligned} e_a &= x_{a\_refe} - x_a \quad \text{and } e_b = x_{b\_refe} - x_b \\ \dot{e}_a &= \dot{x}_{a\_refe} - \dot{x}_a \quad \text{and } \dot{e}_b = \dot{x}_{b\_refe} - \dot{x}_b \end{aligned}\right\} \ldots \tag{36}$$

The objective is to enforce $e_i(t) \rightarrow 0$ such that $x_i(t) \rightarrow x_{i\_ref}(t)$ as $t \rightarrow \infty$, Choosing the design of sliding surface as;

$$s_i = \begin{bmatrix} s_a \\ s_b \end{bmatrix} = \begin{bmatrix} c_1 e_a + \dot{e}_a \\ c_2 e_b + \dot{e}_b \end{bmatrix} \tag{37}$$

Its derivative is $\dot{s}_i = \begin{bmatrix} \dot{s}_a \\ \dot{s}_b \end{bmatrix} = \begin{bmatrix} c_1 \dot{e}_a + \ddot{e}_a \\ c_2 \dot{e}_b + \ddot{e}_b \end{bmatrix}$.

where c_1 and c_2 are design parametres, which is the slope of sliding. e_a and e_b are tracking error of bearing A and bearing B respectively. A Lyapunov function V(x) with the following properties has been selected to ensure convergence to the sliding mode surface:

$$V(x) = \frac{1}{2} S^2(x) \tag{38}$$

In the SMC, the equivalent control, u_{eq}, and the switching control, u_{sw}, make up the control law in most cases. While the switching control compels the system to slide on the sliding surface, the equivalent control maintains the system's status on the sliding surface [17]. One option for an SMC's structure is the one listed in equation (39).

$$u = u_{eq} + u_{sw} = u_{eq} + k\,\text{sign}(S) \tag{39}$$

The derivatives of equation (37) yields

$$\dot{s}_a = -c_1 \dot{x}_a - \ddot{x}_a \quad \text{and } \dot{s}_b = -c_2 \dot{x}_b - \ddot{x}_b \tag{40}$$

$$\dot{s}_a = -c_1 \dot{x}_a - \left(\frac{m_2}{m_1 m_2 - m_3^2} k_{sa} x_a - \frac{m_3}{m_1 m_2 - m_3^2} k_{sb} x_b + \frac{m_2}{m_1 m_2 - m_3^2} k_{ia} i_a - \frac{m_3}{m_1 m_2 - m_3^2} k_{ib} i_b\right) \tag{41}$$

$$\dot{s}_b = -c_2 \dot{x}_b - \left(\frac{-m_3}{m_1 m_2 - m_3^2} k_{sa} x_a + \frac{m_1}{m_1 m_2 - m_3^2} k_{sb} x_b - \frac{m_3}{m_1 m_2 - m_3^2} k_{ia} i_a + \frac{m_1}{m_1 m_2 - m_3^2} k_{ib} i_b\right) \tag{42}$$

The equivalent control, u_{eq}, is derived by solving the first derivative of the sliding function. i.e., $\dot{s}_i = 0$, where the index i reperesents the index bearing a and bearing b.

$$u_{i\_equ} = \begin{bmatrix} u_{a\_equ} \\ u_{b\_equ} \end{bmatrix} \times \begin{bmatrix} \frac{(m_1 m_2 - m_3^2)}{m_2 k_{ia}} \left\{ \begin{aligned} &c_1 \dot{x}_a - \frac{m_2}{m_1 m_2 - m_3^2} k_{sa} x_a \\ &+ \frac{m_3}{m_1 m_2 - m_3^2} k_{sb} x_b \\ &+ \frac{m_3}{m_1 m_2 - m_3^2} k_{ib} i_b \end{aligned} \right\} \\ \frac{m_1 m_2 - m_3^2}{k_{ib} m_1} \left\{ \begin{aligned} &c_2 \dot{x}_b + \frac{m_3}{m_1 m_2 - m_3^2} k_{sa} x_a \\ &- \frac{m_1}{m_1 m_2 - m_3^2} k_{sb} x_b \\ &+ \frac{m_3}{m_1 m_2 - m_3^2} k_{ia} i_a \end{aligned} \right\} \end{bmatrix} \tag{43}$$

By adopting a reaching law with constant rate, $\dot{s} = -k\,sgn(s)\,, k > 0$. The control input becomes

$$u_1 = \frac{(m_1 m_2 - m_3^2)}{m_2 k_{ia}} \left[c_1 \dot{x}_a - \frac{m_2}{m_1 m_2 - m_3^2} k_{sa} x_a + \frac{m_3}{m_1 m_2 - m_3^2} k_{sb} x_b + \frac{m_3}{m_1 m_2 - m_3^2} k_{ib} i_b \right] + k_1 sgn(s_1) \tag{44}$$

$$u_2 = \frac{m_1 m_2 - m_3^2}{k_{ib} m_1} \left[c_2 \dot{x}_b + \frac{m_3}{m_1 m_2 - m_3^2} k_{sa} x_a - \frac{m_1}{m_1 m_2 - m_3^2} k_{sb} x_b + \frac{m_3}{m_1 m_2 - m_3^2} k_{ia} i_a \right] + k_2 sgn(s_2) \tag{45}$$

The stability analysis of the control law has been done and the sliding condition $\dot{v}_1 < 0$ can be satisfied if $\frac{m_2}{m_1 m_2 - m_3^2} k_{ia} * k_1 > 0$ for both AMB a and AMB b.

Therefore, in this paper, fuzzy logic has been applied to replace the switching (reaching) parts of a SMC. In this strategy, a fuzzy interference method substitutes the signum function and tuning terms to smoothen the control operation. The membership functions for input linguistic variable, sliding surface, and output linguistic variable, u_{fuzzy}, are depicted in Fig. 4 and Fig. 5 respectively.

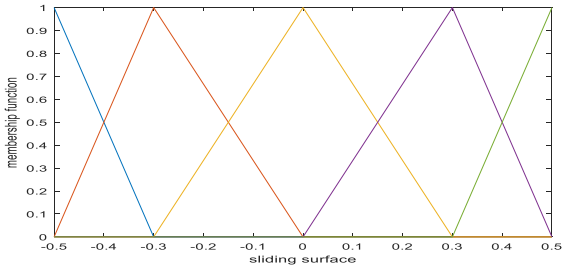

FIGURE 4. Membership function of input lingustic variable.

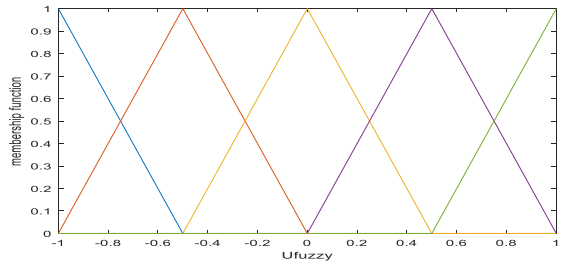

FIGURE 5. Membership function of output lingustic variable.

The linguistic variables of the input and the output are defined as follow.

$$s = [\text{NB} \quad \text{NM} \quad \text{ZERO} \quad \text{PM} \quad \text{PB}]$$
$$u_{fuzzy} = [\text{NB} \quad \text{NM} \quad \text{ZERO} \quad \text{PM} \quad \text{PB}]$$

The Rules of fuzzy logic control formulated in this paper are;

$$R_1 : -If \ \ |s| \ \ is \ NB \ then \ u_{fuzzy} \ is \ NB$$
$$R_2 : -If \ |s| \ \ is \ NM \ \ then \ u_{fuzzy} \ is \ NM$$
$$R_3 : -If \ \ |s| \ \ is \ ZERO \ then \ u_{fuzzy} \ is \ ZERO$$
$$R_4 : -If \ \ |s| \ \ is \ PM \ \ then \ u_{fuzzy} \ is \ PM$$
$$R_5 : -If \ \ |s| \ \ is \ PB \ then \ u_{fuzzy} \ is \ PB$$

Additionally, NN has been used in this paper to enhance the performance of equivalent controller, u_{equ}, by training a parameter of the plant by rapidly estimating unknown parameters to ideal values. The specific steps used for neural network to estimate the unknown parameters are firstly collecting data from the designed Simulink followed by network configuration and selection of the learning algorithm.

TABLE 1. NN model training performance result for control input one, u_1.

Result	Samples	MSE	R
Training	2466	5.53071e-9	9.99999e-1
Validation	529	4.45294e-9	9.99999e-1
Testing	529	4.17500e-9	9.99999e-1

TABLE 2. NN model training performance result for control input two, u_2.

Result	Samples	MSE	R
Training	2466	3.79224e-9	9.99999e-1
Validation	529	2.80442e-9	9.99999e-1
Testing	529	2.12513e-9	9.99999e-1

TABLE 3. Parameter values of AMB system [18].

Parameter	Symbol	Value(unit)
Force displacement stiffness	k_x	16.0533 N/mm
Force current stiffness	k_i	16.0533 N/A
Mass of the rotor	m	13.9 kg
Nominal air gap	x_0	3mm
Bias current	i_0	3A
Permeability of free space	μ	$4\pi x10^{-7}$
Cross sectional area	A	$5.7375*10^{-4} m^2$
Angle of rotation	α	22.5^0
Moment of inertia about x	I	0.0134 kg.m^2
Number of turns	N	269
AMB A's distance from the rotor's center of gravity	a	0.13 m
AMB B's distance from the rotor's center of gravity	b	0.13 m

Selection of tan sigmoidal function for a hidden layer and a pure linear activation function for output layer were one of the major steps. Levenberg – Marquardt type back propagation learning has been used to train the network. As the training performance result, mean square error (MSE) and correction factor (R), is depicted in TABLE 1 for control input 1 and in TABLE 2 for control input 2.

Based on the values gained in Table 1 and Table 2, it is clear to understand the NN perfectly estimates the unknown parameters since the MSE value is very small and the correction factor is very close to one.

The integration of two or more intelligent controllers with SMC offers several advantages, including the ability to compensate for unmodeled dynamics, eliminate chattering, and enhance robustness [19]. In this study, the SMC serves as the primary controller, utilizing the error and derivative of the error as inputs. The Fuzzy logic controller plays a crucial

role by replacing the switching function and tuning the value of the gain, k. Additionally, neural networks are employed to replace the equivalent control and compensate for the unmodeled dynamics. By combining neuro-fuzzy with sliding mode control, the highly chattering problem is effectively eliminated, leading to improved overall system performance [20]. This approach outperforms the sole use of SMC. The overall configuration of the proposed AMB system is given in Fig. 6.

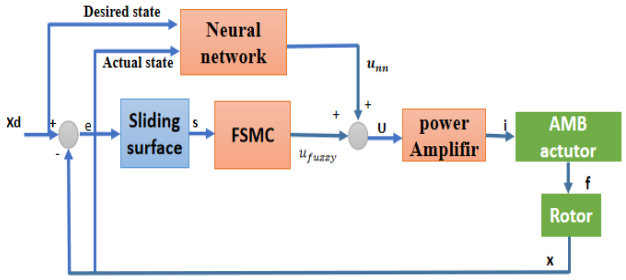

FIGURE 6. Over all configuration of NFSMC for AMB system.

IV. SIMULATION RESULT AND DISCUSSION

To verify the plant model, simulation of the plant without controller has been taken. Fig. 7 and 8 shows the simulation findings for open-loop AMB and closed-loop AMB systems, respectively. The open-loop step response indicates that the system is unstable and exhibits unbounded input-output behavior. Similarly, the closed-loop system without a controller also demonstrates instability and unboundedness. The difference between the two results lies in the settling time and the position value of the rotor. The open-loop step response shows a displacement of 1mm, while the closed-loop response achieves approximately 0.2mm. However, in both cases, the actual values of the rotor position deviate significantly from the nominal values.

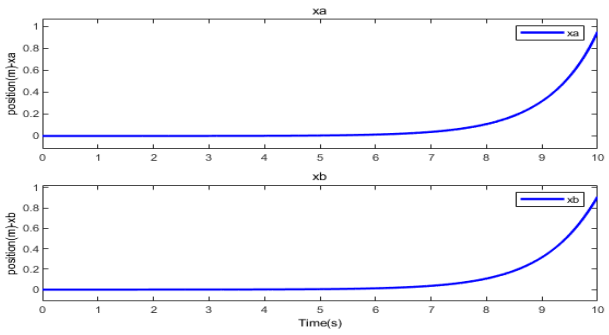

FIGURE 7. Step response of open loop AMB system.

The design parameters for a proposed controller, SMC, has been chosen and selected based on the criteria and approaches in the literature. Table 4. Summarizes the parameters used in the SMC design. As seen from Fig. 9, the rotor positions in bearing A and bearing B closely follow the reference input;

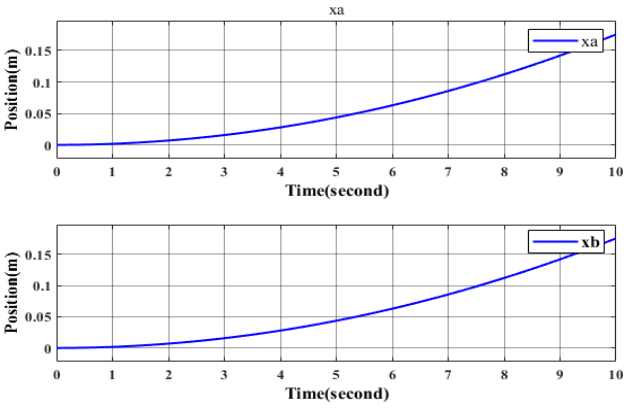

FIGURE 8. Step response of closed loop AMB without controller.

TABLE 4. Designed parameter of the controller.

Controller	Value	
SMC	$c_1 = 15,$ $k_1 = 20,$	$c_2 = 10,$ $k_2 = 10$
FSMC	$c_1 = 15,$ $k_1 = 20,$	$c_2 = 10,$ $k_2 = 10$
NFSMC	$c_1 = 15,$ $k_1 = 20,$	$c_2 = 10,$ $k_2 = 10$

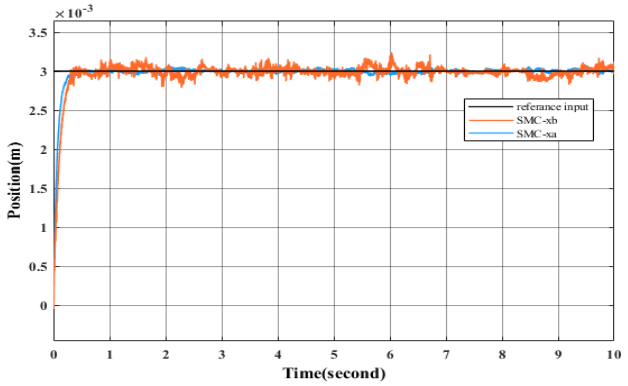

FIGURE 9. Position tracking of SMC based AMB system.

however, they are affected by chattering. The simulation results reveal that the SMC for bearing A exhibits a 0.148 sec. rise time, a 7.5 sec. settling time, and a 8.324% overshoot.

On the other hand, bearing B shows a 0.175 sec. rise time, a 7.5 sec. settling time, and a 9.047% overshoot. In general, the transient response indicates that bearing A exhibits a smaller overshoot, lower rise time, and shorter settling time in comparison to bearing B.

Fig. 9 and 10 clearly demonstrate the effect of chattering, characterized by high-frequency oscillations, on the SMC. Fig. 10 presents the position tracking error plot for AMB A and B. Notably, the tracking performance of SMC is deemed acceptable, as the tracking error remains low.

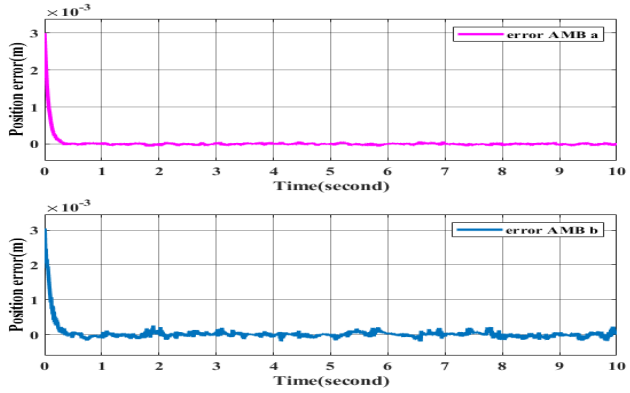

FIGURE 10. Position tracking error.

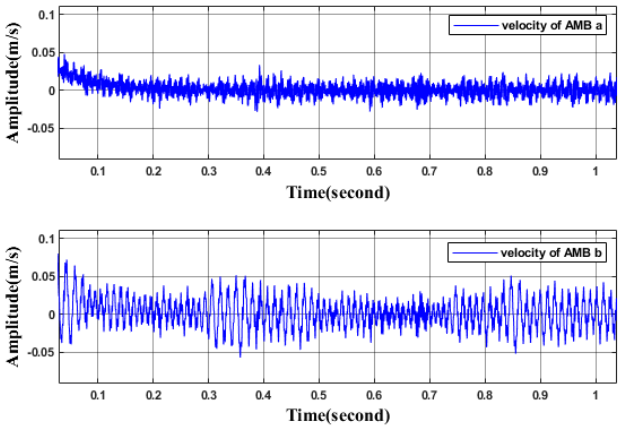

FIGURE 11. Velocity tracking of AMB.

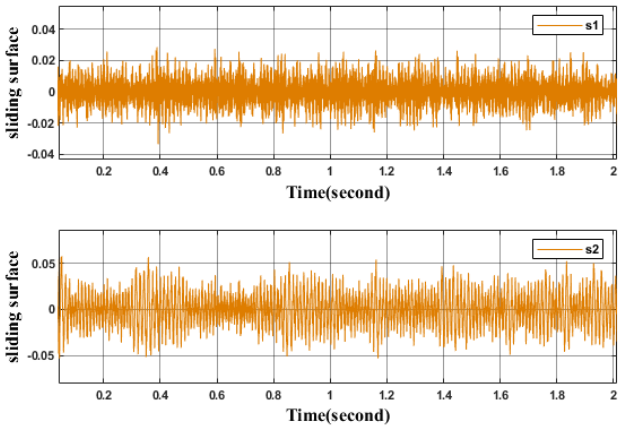

FIGURE 12. Sliding surface of AMB A and AMB B.

Fig. 11 shows the velocity tracking curve of the AMB, where the derivative of the position trajectory has been taken as a velocity trajectory.

From Fig. 9 to Fig. 12, it is evident that the SMC controller exhibits a notable drawback in the form of chattering, which affects all the simulation outputs. Additionally, the methods

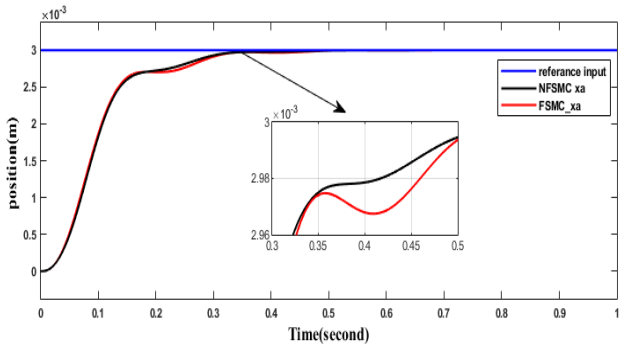

FIGURE 13. Position tracking for FSMC and NFSMC of AMB A system.

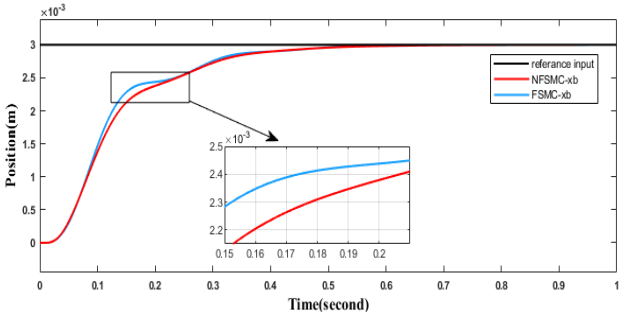

FIGURE 14. Position tracking for FSMC and NFSMC AMB B system.

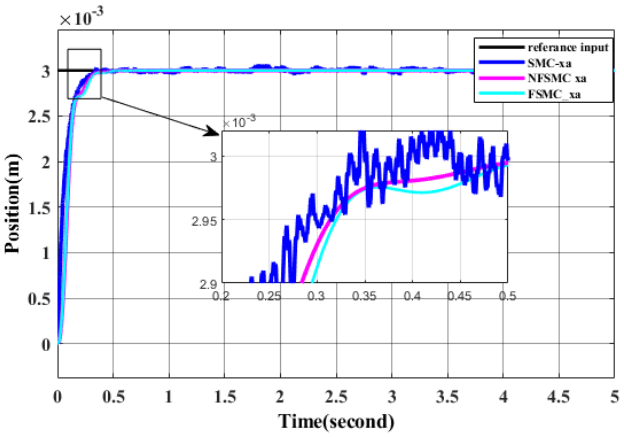

FIGURE 15. Position tracking for SMC, FSMC and NFSMC of AMB A.

of parameter selection for SMC also contribute to this issue. To address and mitigate these drawbacks, this paper introduces NFSMC.

The simulation results presented in Fig. 13 and Fig. 14 reveal that the rotor position operates within the entire feasible region, spanning up to 3 mm. The performance analysis of the system demonstrates that the NFSMC for bearing X_a achieves a 0.1 sec. rise time, a 0.5 sec. settling time, and exhibits no overshoot. Similarly, NFSMC for bearing X_b yields a rise time of 0.12 sec., a settling time of 0.5 sec., and no overshoot is recorded. On the other hand, the FSMC for

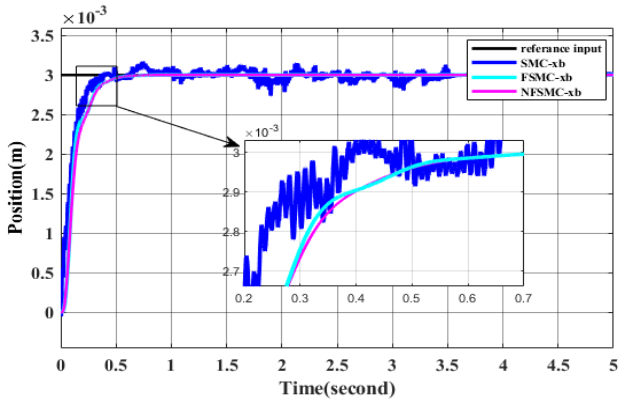

FIGURE 16. Position tracking of SMC, FSMC, and NFSMC of AMB B.

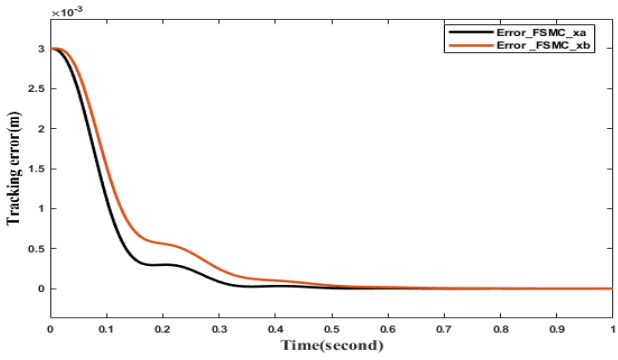

FIGURE 17. Position error tracking of FSMC based AMB system.

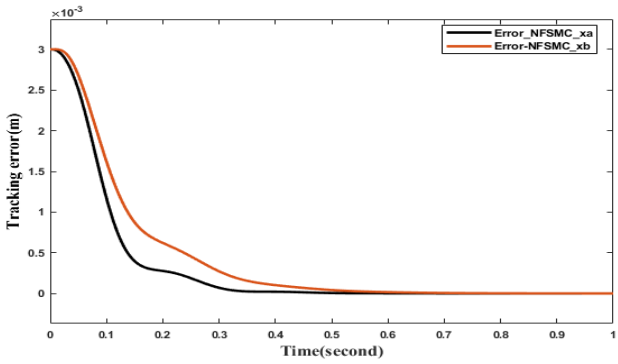

FIGURE 18. Position error tracking of NFSMC based AMB system.

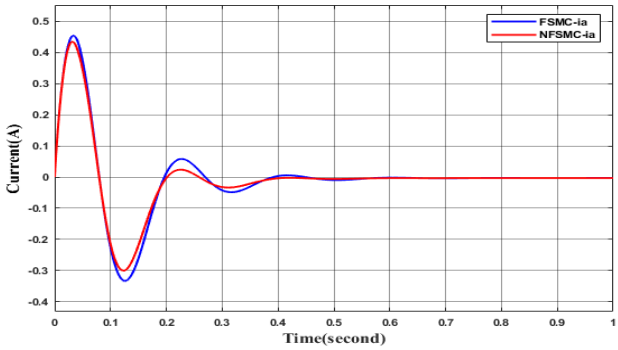

FIGURE 19. Current tracking curve of AMB A system.

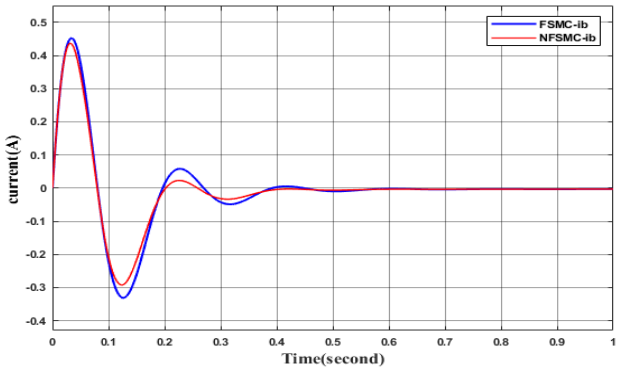

FIGURE 20. Current tracking curve of AMB B system.

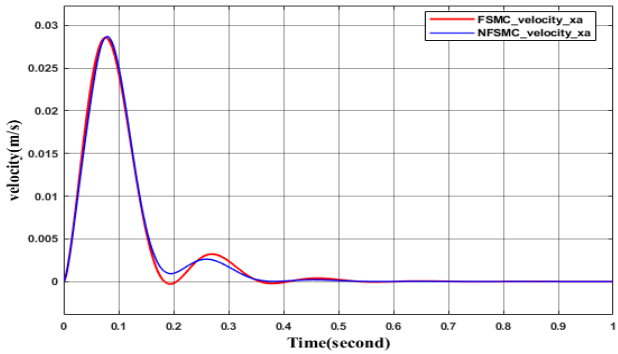

FIGURE 21. Velocity response curve of AMB A system.

bearing X_a demonstrates a 0.123 sec. rise time, a 0.75 sec. settling time, and a 0.464% overshot.

For bearing X_b, FSMC exhibits a rise time of 0.133 sec., a settling time of 0.75 sec., and exhibits a 0.392% overshoot. The rotor can be effectively stabilized at the center of the bearing with a settling time of approximately 0.55 seconds.

Fig. 15 and Fig. 16 clearly shows how SMC is affected by chattering and demonstrate the improved results gained through FSMC and NFSMC. As it is seen from the zoomed version, from 0.2 sec. to 0.5 sec., of Fig. 15 and Fig. 16 the reader can easily understand the result for SMC alone has affected with chattering phenomena in comparison with the results gained through FSMC and NFSMC. Fig. 17 and Fig. 18 illustrate the position error tracking of FSMC and NFSMC for the AMB system, respectively. The results clearly demonstrate that the rotor position accurately follows the reference input, successfully fulfilling the objective of the controller. This indicates that as the system slides along the surface, the error converges to zero over time, even as time approaches infinity.

The simulation results in Fig. 19 and Fig. 20 shown the responses of current tracking curves of bearing A and B. The current in each coil is maintained at the bias current

TABLE 5. Summary on performance analysis of position control of AMB system.

Performance	SMC_xa	SMC_xb	FSMC_xa	FSMC_xb	NFSMC_xa	NFSMC_xb
Rise time	0.148sec	0.17 sec	0.123 sec	0.133 sec	0.1 sec	0.12sec
Settling time	7.5sec	7.5sec	0.75sec	0.75sec	0.5sec	0.5sec
Peak time	1.808 sec	4.132 sec	0.931 sec	0.932 sec	0.737 sec	0.735 sec
Over shoot	8.324%	9.047%	0.464%	0.392%	No	No

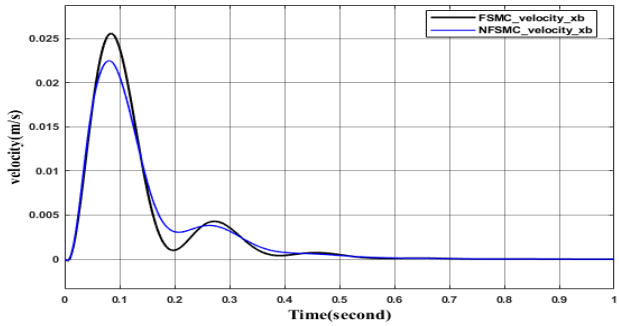

FIGURE 22. Velocity response curve of AMB B system.

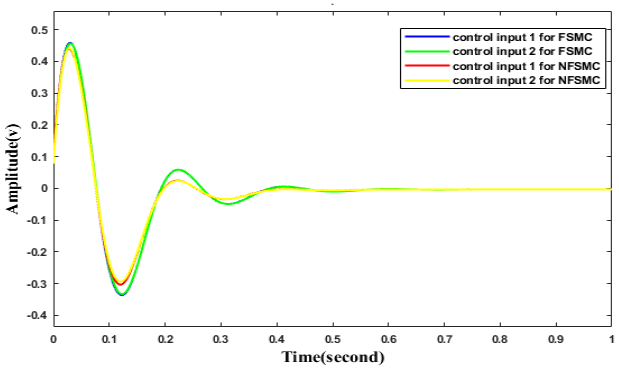

FIGURE 23. Control inputs curve of AMB system.

following the transient time of the displacements. As seen in Fig. 21 and 22 the velocity tracking curves for AMB A and AMB B systems demonstrate that the proposed controller outperforms the FSMC. The proposed controller exhibits minimum overshoot and short settling time in comparison to FSMC based results.

The simulation results depicted in Fig. 23 and Fig. 24 represent the control input and sliding surface for both FSMC and NFSMC based AMB system. These results showcase effective control in maintaining the rotor position, allowing it to rotate freely without contact with the stator. A summary of the transient response performance analysis for position control of AMB system is provided in TABLE 5.

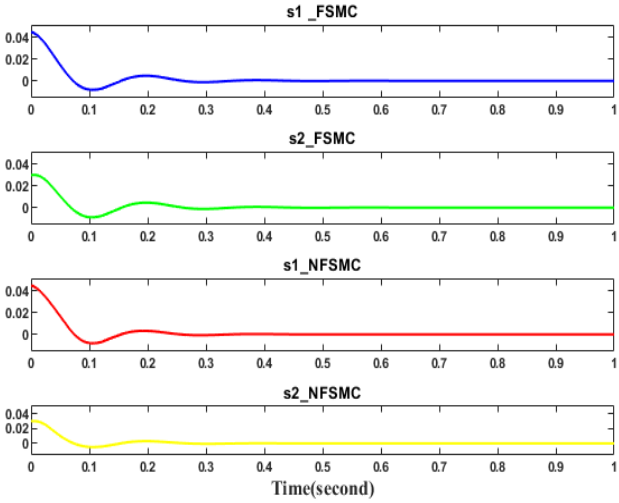

FIGURE 24. Sliding surface for FSMC and NFSMC based AMB system.

V. CONCLUSION

The primary goal of this paper was to show the performance of NFSMC. NFSMC integrates the advantages of NNs, fuzzy logic, and SMC. SMC is known to be susceptible to chattering, which can potentially damage mechanical systems. Thus, the paper proposes the integration of sliding mode control with two intelligent control techniques as a means to address these issues.

As demonstrated in Section IV, the use of SMC for active magnetic bearing systems is affected by chattering. On the other hand, FSMC for AMB system exhibits superior performance compared to SMC. Furthermore, NFSMC proves to be more robust and offers improved system performance when compared to both SMC and FSMC controllers. The results indicate that NFSMC effectively tracks the reference position of the rotor, while the current and velocity simulation results align closely with the nominal values of the plant model. NFSMC significantly reduces overshoot, shortens settling time, accelerates the system response, improves system robustness, and enhances both dynamic and static performance.

In summary, the NFSMC developed in this study offers several advantages, including fast transient response, low overshoot in the dynamic response of system state variables,

reduced settling time, enhanced system robustness, and smoother properties compared to other controllers mentioned here.

REFERENCES

[1] H. Bleuler, "A survey of magnetic levitation and magnetic bearing types," *JSME Int. J.*, vol. 35, no. 3, pp. 335–342, Jan. 1992.
[2] S. Naikwad, "Study active magnetic bearing," *Int. J. Eng. Tech. Res.*, vol. 4, pp. 36–39, Apr. 2016.
[3] T.-J. Su, T.-Y. Li, T.-Y. Tsou, V.-N. Giap, and Q.-D. Nguyen, "Proportional–integral–derivative/fuzzy sliding mode control for suspension of active magnetic bearing system," *Adv. Mech. Eng.*, vol. 9, no. 12, pp. 1–8, Dec. 2017.
[4] S. M. Raafat, S. A. Al-Samarraie, and A. M. Mahmood, "Unity sliding mode controller design for active magnetic bearings system," *J. Eng.*, vol. 21, no. 6, pp. 90–107, Jun. 2015.
[5] G. P. Incremona, M. Rubagotti, and A. Ferrara, "Sliding mode control of constrained nonlinear systems," *IEEE Trans. Autom. Control*, vol. 62, no. 6, pp. 2965–2972, Jun. 2017.
[6] X. Wang, Y. Zhang, and P. Gao, "Design and analysis of second-order sliding mode controller for active magnetic bearing," *Energies*, vol. 13, pp. 1–14, Nov. 2020.
[7] Z. Cao, J. Dong, F. Wani, H. Polinder, P. Bauer, F. Peng, and Y. Huang, "Sliding mode control with neural network for active magnetic bearing system," in *Proc. 45th Annu. Conf. IEEE Ind. Electron. Soc. (IECON)*, vol. 1, Oct. 2019, pp. 744–749.
[8] H.-K. Chiang, C.-T. Chu, and Y.-T. Jhoui, "Fuzzy control with fuzzy basis function neural network in magnetic bearing system," *Ind. Electron.*, vol. 12, pp. 846–851, May 2012.
[9] D. Shiferaw and R. Mitra, "Neuro-fuzzy sliding mode controller: Design and stability analysis," *Int. J. Comput. Intell. Stud.*, vol. 1, no. 3, pp. 242–255, Sep. 2010.
[10] C.-F. Hsu, T.-T. Lee, C.-M. Lin, and L.-Y. Chen, "Robust neuro-fuzzy controller design via sliding-mode approach," in *Proc. IEEE Int. Conf. Fuzzy Syst.*, vol. 2, Jul. 2004, pp. 917–922.
[11] A. Boubakir, F. Boudjema, and S. Labiod, "A neuro-fuzzy-sliding mode controller using nonlinear sliding surface applied to the coupled tanks system," *Int. J. Autom. Comput.*, vol. 6, no. 1, pp. 72–80, Feb. 2009.
[12] S. A. Khader, "System identification of active magnetic bearing for commissioning," UPPSASA Universities, Uppsala, Sweden, Tech. Rep., no. 1, pp. 289–294, Jan. 2015.
[13] E. A. Workeye, T. G. G/Meskel, and Y. K. T/Himanot, "Design of genetic algorithm based robust LQG controller for active magnetic bearing system," *Adv. Sci. Technol.*, vol. 411, pp. 215–236, Jan. 2022.
[14] S. Madhura and T. V. Govindaraju, "Design and testing of an active magnetic bearing," *Int. J. Advance Res. Sci. Eng.*, vol. 6, no. 10, pp. 257–263, Oct. 2017.
[15] A. Noshadi, J. Shi, W. S. Lee, P. Shi, and A. Kalam, "System identification and robust control of multi-input multi-output active magnetic bearing systems," *IEEE Trans. Control Syst. Technol.*, vol. 24, no. 4, pp. 1227–1239, Jul. 2016.
[16] F. Z. Daikh and M. F. Khelfi, "Sliding mode with neuro-fuzzy network controller for inverted pendulum," *Int. J. Autom. Control*, vol. 9, no. 1, p. 24, 2015.
[17] J. Liu and X. Wang, *Advanced Sliding Mode Control for Mechanical Systems*. Beijing, China: Springer-Verlag, Dec. 2011.
[18] A. R. Husain, M. N. Ahmad, and A. H. M. Yatim, "Deterministic models of an active magnetic bearing system," *J. Comput.*, vol. 2, no. 8, pp. 9–17, Oct. 2007.
[19] L. Ouada, S. Benaggoune, and S. Belkacem, "Neuro-fuzzy sliding mode controller based on a brushless doubly fed induction generator," *Int. J. Eng.*, vol. 33, no. 2, pp. 248–256, Feb. 2020.
[20] Z. Tang, "Control design for the active magnetic bearing system," Ph.D. dissertation, Fac. Sci. Eng., Univ. Manchester, Manchester, U.K., Jun. 2019.

HAREGEWOYN FENTAW ASRES received the B.Sc. degree in electrical and computer engineering (industrial control engineering) from Hawassa University, Hawassa, Ethiopia, in 2017, and the M.Sc. degree in electrical and computer engineering (control system engineering) from Bahir Dar University, Bahir Dar, Ethiopia, in 2023. She is currently a Lecturer with the Woldia Institute of Technology, Woldia University. Her research interests include space vehicles, intelligent systems, renewable energy, and automation.

ABRHAM TADESSE KASSIE received the B.Sc. degree in electrical and computer engineering (industrial control engineering) from Hawassa University, Hawassa, Ethiopia, in 2015, and the M.Sc. degree in electrical and computer engineering (control and instrumentation engineering) from Addis Ababa Science and Technology University, Addis Ababa, Ethiopia, in 2019. He is currently a Senior Lecturer with the Bahir Dar Institute of Technology, Bahir Dar University. He serves as the Chair for the Control and Instrumentation Engineering, Bahir Dar Institute of Technology. He has been involved in more than five community services, two technology transfers, and two mega projects. Additionally, he has published two articles in the Scopus Web of Science Journals. His research interests include robotics, electric vehicles, renewable energy, artificial intelligent, and machine learning.